ELSEVIER

Journal of Nuclear Materials 318 (2003) 113–121

journal of nuclear materials

www.elsevier.com/locate/jnucmat

Bubble dynamics in the thermal shock problem of the liquid metal target

S. Ishikura [a,*], H. Kogawa [a], M. Futakawa [a], K. Kikuchi [a], R. Hino [a], C. Arakawa [b]

[a] *Japan Atomic Energy Research Institute, Tokai-mura, Ibaraki-ken 319-1195, Japan*
[b] *University of Tokyo, Bunkyo-ku, Tokyo 113-8656, Japan*

Abstract

The thermal shock stress in a mercury target vessel was analyzed. The target receives the incident proton beam at an energy of 1 MW with a pulse duration of 1 μs. A negative pressure of 61 MPa was generated following the dispersion of the compression field at 52 MPa which was generated by the proton beam injection. It is expected that cavitation may be caused by the negative pressure. In order to evaluate the cavitation behavior and the following material damage mechanism, a simulation study was carried out using the equation of motion based on bubble dynamics for a single bubble, and fundamental parameter analysis was carried out. It is found that a bubble has a volume expansion of more than 1000 times with a change of the pressure at the window of the target vessel. Consequently wave propagation will be affected. Theoretical consideration was given to the wave motion of propagation in a bubbly liquid. The equation of state in a bubbly liquid can be approximated by polynomials. The diameter of a bubble and the bubble volume fraction inherent in mercury can be estimated if the critical pressure, the sound velocity, and resonance frequency are measured by static and dynamic experiments.

1. Introduction

The Japan Atomic Energy Research Institute (JAERI) and the High Energy Accelerator Research Organization (KEK) have cooperatively promoted a plan for constructing a neutron scattering experiment facility of MW scale using a high intensity proton accelerator. Liquid mercury is to be used for the target as a spallation neutron source. The structure of this target is shown in Fig. 1. The power of the proton beam is 1 MW:3 GeV and 333 μA. The pulse duration of the beam is 1 μs, and a repetition rate 25 Hz. The proton beam passes through the window of the target vessel and interacts with a mercury target. The high energy density deposited in mercury generates heat. Consequently a pressure wave occurs inside the target. This pressure wave has a possibility of damaging the internal wall of the target window. Fig. 2 shows an example of the analytical results of pressure change in mercury generated by the pressure wave [1]. In this analysis, mercury is assumed to be an elastic body. The mercury near the window of the target vessel, a negative pressure of 3.7 MPa arises after proton beam incidence. The negative pressure means that mercury is not compressed but expanded. This is caused by the dynamic interaction of the target vessel and mercury. It is expected that cavitation may be caused by the negative pressure. In order to evaluate the cavitation behavior and the following material damage mechanism, a simulation study was carried out using the equation of motion based on bubble dynamics for a single bubble, and fundamental parameter analysis was carried out.

The experiment on the negative pressure in mercury was done by Briggs [2]. They treated mercury by means of vacuuming, torching and heating in a furnace at various temperatures in order to degas mercury. Then

* Corresponding author. Tel.: +81-29 282 5058; fax: +81-29 282 6489.
E-mail addresses: ishikura@cat.tokai.jaeri.go.jp (S. Ishikura), kikuchi@popsvr.tokai.jaeri.go.jp (K. Kikuchi).

0022-3115/03/$ - see front matter © 2003 Elsevier Science B.V. All rights reserved.
doi:10.1016/S0022-3115(03)00086-2

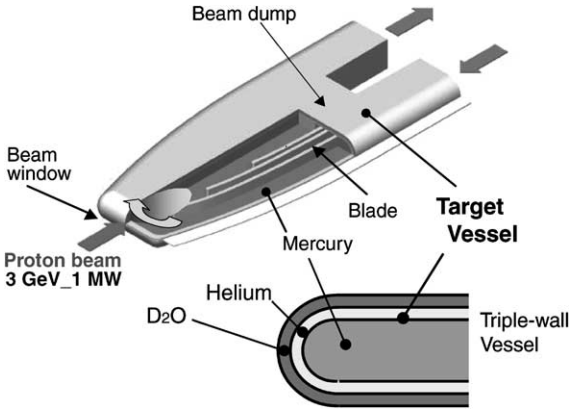

Fig. 1. Schematic drawing of the structure of mercury target vessel.

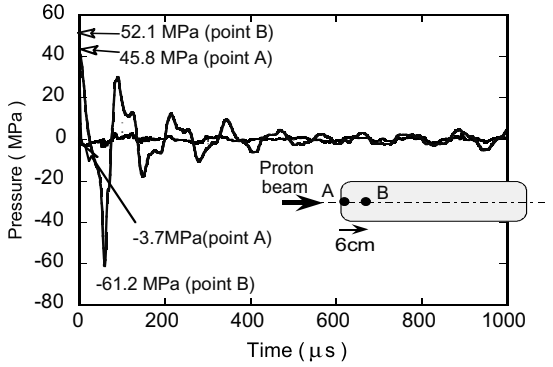

Fig. 2. Analytical pressure response at top window.

centrifugal force was applied to the mercury in a Pyrex glass tube. The negative pressure threshold for cavitation depended very much on the preparation of mercury; it was 0.7 MPa after vacuum processing, 4.6 MPa after torching process and 4.7–42.5 MPa after heating in a furnace, respectively. The negative pressure threshold increased with increasing furnace temperature.

In the target design, the negative pressure reaches the maximum of about 60 MPa at a time of 60 μs in the area 6 cm away from the window, noted by the point B. The occurrence of a negative pressure in mercury has suggested the possibility that cavitation will occur. As a result, the propagation characteristics of the pressure wave may change and the vessel material in contact with mercury may receive damage.

In this paper, the behavior of the pressure wave under the condition of gas bubbles existence, which spreads in mercury, is analyzed. The dynamic equation of motion for the case that a gas bubble exists in mercury is derived. Then, this equation is extended into mercury with a large number of gas bubbles. Furthermore, the result of the propagating pressure wave in mercury is considered. A design technique to estimate the size of bubbles and the volume fraction inherent in mercury is proposed finally.

2. Dynamics of single bubble

In order to predict the dynamic behavior of a single bubble, a mathematical model based on the dynamics of a gas bubble is considered [3]. This dynamics explains the motion of a gas bubble in response to the changes of the pressure in the liquid containing the gas bubble. The existence of the bubble, which is presumably caused by cavitation, is assumed.

2.1. Static equilibrium equation

Consider the case that a gas bubble with a radius of R exists in the liquid with a static pressure of P_0. Static balance of the pressure is expressed by Eq. (1). As shown in Fig. 3, the liquid pressure $P_B(r > R)$ near the bubble balances the pressure in the bubble P_i and the pressure P_σ corresponding to the surface tension at the bubble interface.

$$P_B = P_i - P_\sigma, \quad P_i = P_g + P_v, \tag{1}$$

where P_v is the vapor pressure and P_g is the gas pressure in the bubble. P is calculated from the state of an initial bubble $(R = R_0)$ expressed by Eq. (2).

$$P_g = \left(P_0 + \frac{2\sigma}{R_0} - P_v\right)\left(\frac{R_0}{R}\right)^{3\gamma}, \tag{2}$$

where γ is the specific heat ratio, which is 1.402 for air. Substituting Eq. (2) into Eq. (1) gives Eq. (3).

$$P_B = \left(P_0 + \frac{2\sigma}{R_0} - P_v\right)\left(\frac{R_0}{R}\right)^{3\gamma} + P_v - \frac{2\sigma}{R}. \tag{3}$$

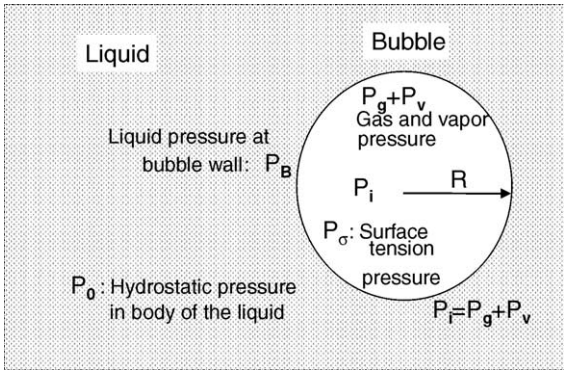

Fig. 3. Pressure balance of a gas bubble which exists in liquid.

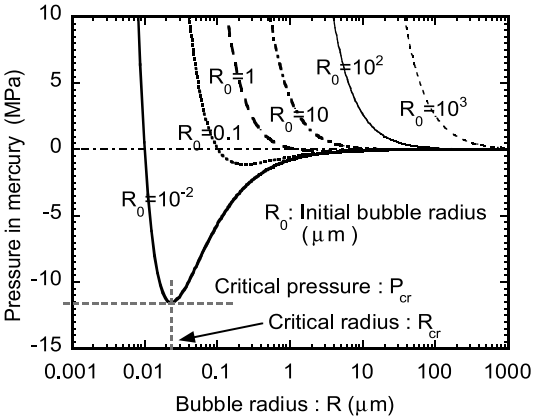

Fig. 4. Relation of pressure to initial bubble radius.

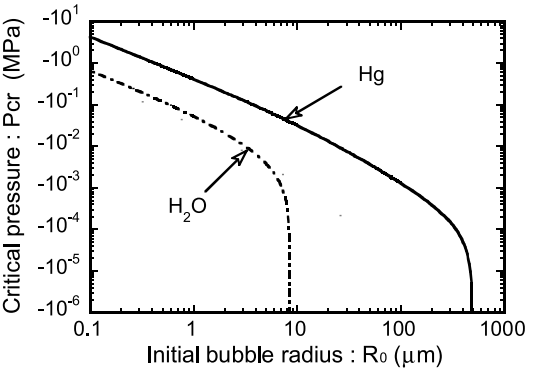

Fig. 5. Critical pressure to the initial bubble radius.

Fig. 4 shows the relation of the pressure in mercury to the radius of a bubble at the initial size of R_0. The static pressure in the liquid mercury is assumed to be atmospheric pressure ($P_0 = 0.1$ MPa). The values of the physical properties in mercury used for calculations are shown in Table 1. If the pressure in mercury is reduced, the volume of the bubble expands. If the bubble is shrunk to its critical point it becomes statically unstable. An inertia force will exist below the critical point, but it will not happen in the quasi-static state. This critical point is the generating condition for cavitation. The critical radius R_{cr} and the critical pressure P_{cr} of liquid at the critical point can be obtained by setting the partial differential coefficient of Eq. (3) to zero. There is a tendency for P_{cr} to become low as the diameter of bubble becomes small, which means that cavitation does not generate easily. As mentioned in Briggs' experiment [2], careful degassing of mercury showed large negative pressure thresholds for cavitation. It is thought that this degassing process removed large size bubbles in mercury.

Fig. 5 shows the relation between the critical pressure and the initial radius of bubble. For mercury, the critical pressure decreases with increasing bubble radius up to 100 μm. Above 100 μm the critical pressure decreases abruptly, especially, when at the time bubble radius becomes 500 μm. In water, the critical pressure falls abruptly at a bubble radius of about 10 μm. Therefore, in static equilibrium conditions, critical (negative) pressure of a bubble is smaller at large initial bubble radii.

Table 1
Material properties

Items	Water	Mercury	Air
Density, ρ (kg/m^3)	996.6	13 528	1.18
Bulk modulus, K_s (GPa)	2.16	25.5	–
Surface tension, σ (Pa)	0.0717	0.47	–
Vapor pressure, P_v (Pa)	3530	0.28	–
Shear viscosity, μ (mPa s)	0.854	1.52	–
Thermal conductivity, K (W/m K^{-1})	0.61	8.52	0.026
Specific heat, c_p (kJ/kg K^{-1})	4.179	0.139	1.01

2.2. The basic equation of single bubble motion about expansion and contraction

Regarding the derivation of the equation of motion for a single bubble, reports by Fujikawa and Akamatsu [4] and Matsumoto and coworkers [5] consider the substance movement by evaporation and condensation on a bubble boundary. In this research, however, in order to use of a general-purpose computer code, the method of Prosperetti et al. [6] is applied. This method solves three equations simultaneously that consists of Eq. (4), which is the Keller's equation with the consideration of compressibility in the liquid, the Eqs. (5) and (6), which are the formula of pressure and temperature with consideration to the mass conservation and the energy conservation rules of the gas in the bubble, respectively.

The momentum equation is given by

$$\left(1-\frac{\dot{R}}{c}\right)R\ddot{R}+\frac{3}{2}\left(1-\frac{\dot{R}}{3c}\right)\dot{R}^2 = \frac{1}{\rho_L}\left(1+\frac{\dot{R}}{c}\right)\left[P_B(t)-P_0-P_s\left(t+\frac{R}{c}\right)\right]+\frac{R}{\rho_L c}\frac{dP_B(t)}{dt}$$

$$P_i(t)=P_B(R,t)+2\sigma/R+4\mu_L\dot{R}/R. \tag{4}$$

The force balance equation is given by

$$\frac{dP_i}{dt}=\frac{3}{R}\left((\gamma-1)K\frac{\partial T}{\partial r}\bigg|_R-\gamma P_i\dot{R}\right). \tag{5}$$

The energy equation is given by

$$\frac{\gamma}{\gamma-1}\frac{P_i}{T}\left(\frac{\partial T}{\partial t}+u\frac{\partial T}{\partial r}\right)-\frac{\mathrm{d}P_i}{\mathrm{d}t}=\nabla\cdot(K\nabla T), \tag{6}$$

where $\dot{R}$ is the time differential of bubble radius R, c the sound velocity in a liquid, ρ_L the density, μ_L the coefficient of viscosity, σ the surface tension, $P_i(t)$ the inner pressure of bubble, P_0 the static pressure in liquid, $P_s(t)$ the pressure oscillation near the bubble, $P_B(t)$ the pressure of liquid at the bubble perimeter, T the temperature in a bubble, u the gas flow velocity in a bubble, γ the ratio of specific heat, and K the thermal conductivity of the gas in the bubble.

2.3. Resonance frequency of bubble

Prosperetti et al. consider the case of small-amplitude oscillations of a bubble for the linearization. Neglecting the compressibility term of Eq. (4), which means Rayleigh–Plesset equation, a resonant frequency ω_0 of a single bubble can be derived by Eq. (7).

$$\omega_0=\sqrt{\frac{P_0}{\rho_L R_0^2}\left(\mathrm{Re}[\Phi]-\frac{2\sigma}{R_0P_0}\right)}, \tag{7}$$

where ρ_L is the density of a liquid, and $\mathrm{Re}[\phi]$ the real part of a complex number that is given from the energy conservation rule. Fig. 6 shows the relation between the radius of an initial bubble and the resonance frequency of bubble in mercury. The approximate solution, for the case omitting the surface tension of the mercury, is also shown in the figure. Above a 10 μm radius of the bubble, the exact solution is well matched with the approximate solution. However, the difference of resonance frequency becomes large if the surface tension of the mercury is taken into consideration below 10 μm. As shown in Fig. 2, the frequency of pressure change in mercury near the target vessel tip is nearly 9 kHz. The initial bubble radius equivalent to this frequency is 90 μm.

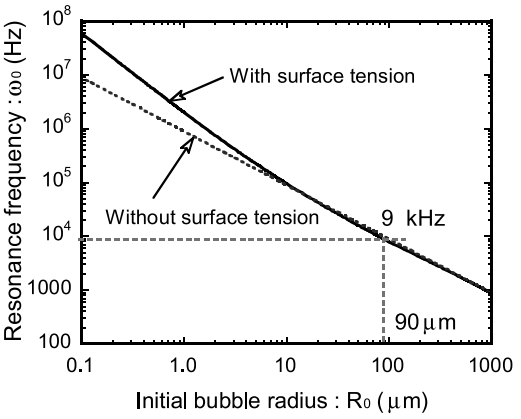

Fig. 6. Resonance frequency vs. initial bubble radius.

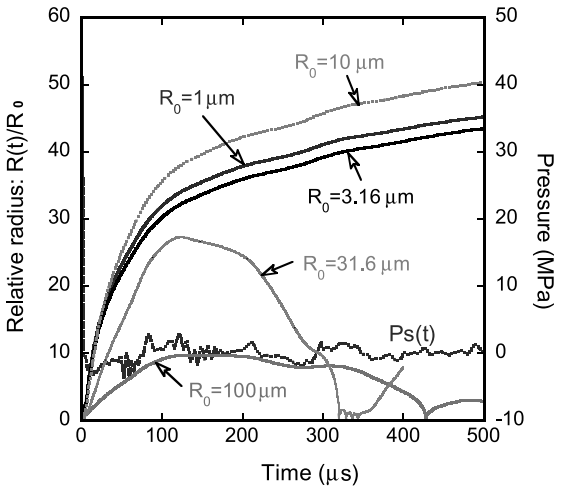

Fig. 7. Bubble response for the pressure wave at the window of a target container.

2.4. Dynamics of single bubble

The simulation of the dynamic motion of a single bubble was performed. The method of numerical solution was the Rational-Runge–Kutta [7] for the Eqs. (4)–(6). The frequency response characteristic of a single bubble has been reported [1]. The pressure change P_s of the liquid surrounding the bubble equivalent to the pressure history at the tip of the target window, as shown in Fig. 2, is considered.

The calculated motion of a bubble is shown in Fig. 7 for initial bubble radii of 1, 3.16, 10, 31.6 and 100 μm, respectively. When the radius of an initial bubble ranges between 1 and 10 μm, the bubble begins to expand simultaneously with the early generation of negative pressure. The bubble grows 40–50 times its initial size, and the state is maintained during several 100 μs.

The relative radius will become 30 times for $R_0 = 31.6$ μm. The relative radii of expansion falls about 10 times for $R_0 = 100$ μm. However, the period of bubble expansion is within several 100 μs. There is not very much difference between these two cases from the viewpoint of volume expansion. In each case the relative radius increases more than 10 times, in another word the volume expands by a factor of more than 1000.

3. Dynamics of bubbly liquid

3.1. Effect of bubble volume fraction

The wave propagation in a bubbly liquid was treated using the equivalent sound velocity obtained from the relation between the mixed density of gas in liquid and

the pressure. For the case where the interaction of bubbles can be disregarded the volume fraction, β, is small ($\beta < 10^{-3}$). Foldy [8] formulated the sound velocity in a bubbly liquid. The scattering theory with consideration to the dynamic action of each bubble was used, assuming that the bubbles were the rigid spheres.

Van Wijjngaarden [9] introduced the same formula with the result of Foldy, by solving the Euler equation for two-phase flows and the Rayleigh–Plesset equation that is the dynamic equation for a single bubble. Caflisch et al. [10] proved that the result of Wijjngaarden was right as a result of performing theoretical deployment. In addition, there are some techniques for deriving the equation of motion for a bubble group from a single bubble. Prosperetti and coworkers [11,12] used the equation of Keller [6] that gave an expression the equation of the motion for a single bubble. We also use this technique. In the next paragraph, the wave motion equation in the bubbly liquid is calculated by the technique of Prosperetti. The derived equation for the sound velocity is shown.

The mass conservation and Euler's equation of motion in liquid whose bubble volume fraction is β are expressed by the Eqs. (8) and (9).

$$\frac{1}{\rho_L c_0^2}\frac{\partial P}{\partial t} + \nabla \cdot u = \frac{\partial \beta}{\partial t},$$
$$\beta(x,t) = \frac{4}{3}\pi \int R^3(a;x,t) f(a;x)\,\mathrm{d}a,$$
$$n = \int f(a;x)\,\mathrm{d}a, \tag{8}$$

$$\rho_L \frac{\partial u}{\partial t} + \nabla P = 0, \tag{9}$$

where P is the pressure, u the velocity of the bubbly liquid, c_0 the sound velocity in the normal liquid, $\beta(t)$ the bubble volume fraction when n bubbles with the same size exist, $\beta(x,t)$ the bubble volume fraction when a distribution function, $R(a;x,t)$ denotes the radius at time t of a bubble located at position x and having an bubble radius a, $f(a;x)$, defines the bubble probability distribution in the coordinate x and bubble radius, a. When the change of both the sound velocity and the density is small, the linear equation of the wave motion containing a change of the rate of bubble volume can be obtained by Eq. (10)

$$\frac{1}{c_0^2}\frac{\partial^2 P}{\partial t^2} - \nabla^2 P = \rho \frac{\partial^2 \beta}{\partial t^2}. \tag{10}$$

Using the dynamic Eqs. (4)–(6) combined with Eq. (10), the rate of change of bubble volume and bubble radius R are solved simultaneously. Thus, the wave motion phenomenon in bubbly liquid can be solved.

In order to understand the basic characteristic of the wave motion phenomenon in a bubbly liquid, a small oscillating domain with weak nonlinearity is considered. The dynamic Eqs. (4)–(6) are linearlized about the nonlinear term of bubble radius and are substituted into Eq. (10). Then the equation of dispersion for a standing wave is given by Eq. (11).

$$k_m^2 = \frac{\omega^2}{c_0^2} + 4\pi\omega^2 \int_0^\infty \frac{a f(a)\,\mathrm{d}a}{\omega_0^2 - \omega^2 - 2\mathrm{i}b\omega}, \tag{11}$$

where k_m is the number of waves, b the complex attenuation, ω the frequency of pressure oscillation in the liquid, a the radius of bubble, $f(a)$ the distribution of bubble radius. Furthermore, if the bubble distribution is assumed to be homogeneous with an average radius of $\bar{a}$ and n bubbles per unit volume, then Eq. (12) is given from Eq. (11).

$$\frac{c_0^2}{c_m^2} = 1 + \frac{4\pi c_0^2 n \bar{a}}{\omega_0^2 - \omega^2 - 2\mathrm{i}b\omega}, \tag{12}$$

where c_m is the relative sound velocity in bubbly liquid. Fig. 8 shows the results of the relative sound velocity as a function of frequency. In the analysis, the initial radius of bubble (R_0) is 1 μm and the initial void fraction (β_0) is 10^{-4}. The relative sound velocity is normalized by the sound velocity without bubbles. Below the resonance frequency of the bubble at the lower frequency regime, the relative sound velocity becomes lower than that without bubbles. In the higher frequency regime, the relative sound velocity close to unity are obtained.

Fig. 9 shows the relative sound velocity in the low frequency regime for a bubbly liquid at various initial radii. When the bubble volume fraction becomes 10^{-6}, then the relative sound velocity begins to decrease. For the case of 1 μm initial bubble radius, it decreases by half at 10^{-4} bubble volume fraction. Clearly, the sound velocity is affected by the existence of the bubbles. If a critical pressure and sound velocity are measured in the

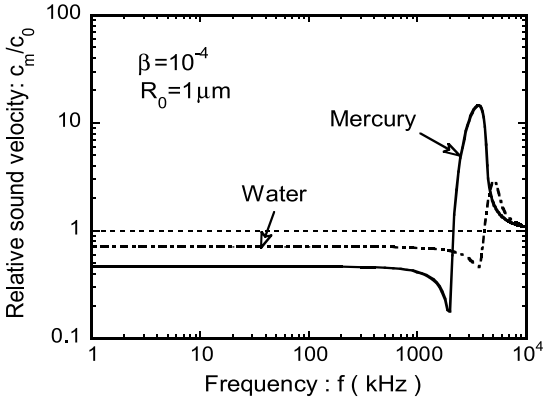

Fig. 8. Relative sound velocity in bubbly liquid.

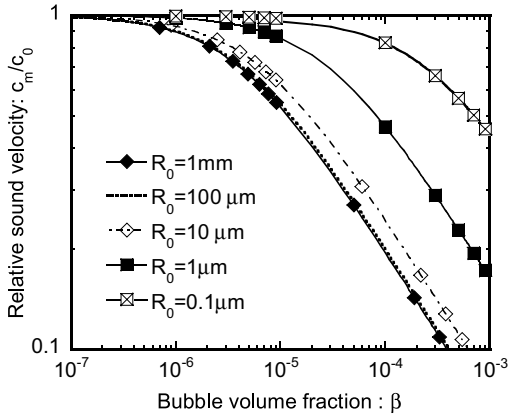

Fig. 9. Relative sound velocities of bubbly liquids below the resonant frequencies for various initial bubble radii.

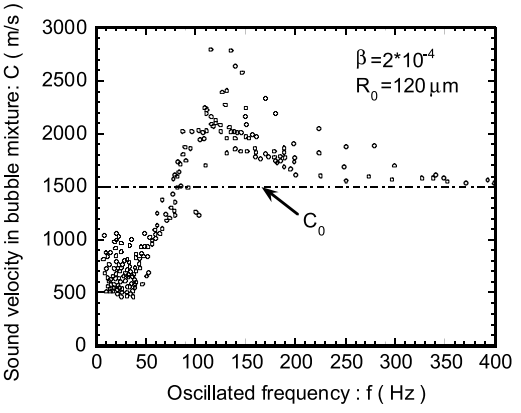

Fig. 10. Experimentally determined sound velocities in bubbly water by Fox et al. [13].

static and dynamic experiments, respectively, the bubble radius and the bubble volume fraction can be estimated using the Eqs. (3), (7) and (12). Fig. 10 shows the sound velocity in water measured by Fox et al. [13]. The sound velocity in bubbly water was reduced below 1500 m/s at the lower frequency but increased more than that at the high frequency.

3.2. Nonlinear wave equation in bubbly liquid

It is difficult to solve the dynamic equations of motion using the Eqs. (4)–(6) with Eq. (10) simultaneously. Especially for the design work for a spallation target, one possible way is to use commercial finite element method (FEM) code like LS-DYNA [18] or ABAQUS [19], for example. But it is not so practical because lots of works must be done to modify them to simulate the wave motion in a bubbly liquid. Eq. (4) was derived in terms of bubble radius R. On the other hand, another expression in bubble dynamics was given for the bubble volume [14,15].

$$\ddot{v} + \delta\omega_0\dot{v} + \eta p = av^2 + b(2v\ddot{v} + \dot{v}^2), \tag{13}$$

where v is the bubble volume, $\delta(=4\mu/\omega_0 R_0^2)$ the viscous damping coefficient, μ the kinematic viscosity, $\eta = 4\pi R_0/\rho_0$, $a = (\gamma+1)\omega_0^2/2V_0$, γ the ratio of specific heats, $b = 1/6V_0$, V_0 the initial bubble volume.

The frequency of pressure in the mercury target fluctuates around 9 kHz as shown in Figs. 2 and 7, although the resonance frequency of bubbles in mercury is estimated to be on the order over the 100 kHz. Here, we consider the low frequency region whose dominant frequency components satisfy the relation $\omega^2 \ll \omega_0^2$. Therefore, the first nonlinear term in Eq. (13) dominates the second at the low frequencies. Thus Eq. (14) was obtained.

$$v = -\frac{\eta}{\omega_0^2}p - \frac{\delta}{\omega_0}\dot{v} - \frac{1}{\omega_0^2}\ddot{v} + \frac{a}{\omega_0^2}v^2, \quad \omega^2 \ll \omega_0^2. \tag{14}$$

Further approximation by $v = -\eta p/\omega_0^2$ gives Eq. (15)

$$v = -\frac{\eta}{\omega_0^2}p - \frac{\delta\eta}{\omega_0^3}\dot{p} - \frac{\eta}{\omega_0^4}\ddot{p} + \frac{a\eta^2}{\omega_0^6}p^2. \tag{15}$$

As β in Eq. (8) is given by $n \times v$ where β is the bubble volume fraction, n the number of bubbles, v the bubble volume, Eq. (16) is given by merging Eq. (10) with Eq. (15) and omitting derivative terms in the pressure fluctuation higher than third order.

$$\left(\frac{1}{c_0^2} + \frac{\rho_0\beta_0}{\gamma p_0}\right)\frac{\partial^2 P}{\partial t^2} - \nabla^2 P = \frac{(\gamma+1)\rho_0\beta_0}{2\gamma^2 p_0^2}\frac{\partial^2 P^2}{\partial t^2}, \tag{16}$$

where Eq. (16) is equivalent to Eq. (17) that was given by Westervelt [17] without the dissipation term on the nonlinear acoustics.

$$\frac{1}{c_0^2}\frac{\partial^2 P}{\partial t^2} - \nabla^2 P = \frac{\varepsilon}{\rho_0 c_0^4}\frac{\partial^2 P^2}{\partial t^2}, \tag{17}$$

where ε is a nonlinear parameter defined by the ratio of the first order to the second order terms in Taylor series of the equation of state (EOS) [16].

Equating the coefficients for each corresponding term in the Eqs. (16) and (17), the nonlinear-wave equation for a bubbly liquid is given by the Westrvelt equation which is the governing Eq. (18) in terms of the equivalent sound velocity and the nonlinear parameters.

$$\frac{1}{\bar{c}_0^2} = \left(\frac{1}{c_0^2} + \frac{\rho_0\beta_0}{\gamma p_0}\right), \quad \frac{\bar{\varepsilon}}{\rho_0\bar{c}_0^4} = \frac{(\gamma+1)\rho_0\beta_0}{2\gamma^2 p_0^2}, \tag{18}$$

where the top bar on $\bar{\varepsilon}$ and $\bar{c}$ denoted the expression for a bubbly liquid. This shows that the EOS based on polynomials can simulate the wave propagation of the bubbly liquid. This means that commercial FEM or fi-

nite difference method (FDM) codes which can use polynomial EOS (namely, nonlinear parameter ε) are valid for use in our study.

3.3. Nonlinearity of bubbly liquid

The nonlinearity of the bubbly liquid is considered by varying the initial radius or the volume fraction of the potential bubble in mercury and in water. Although the surface tension is not considered in Eq. (16), the effect of the surface tension in mercury is large, as mentioned in the Section 2. Hence, in order to apply the surface tension to mercury, we considered it in Eq. (13). Accordingly, the nonlinear parameter of bubbly liquid, which considered the surface tension, was obtained by the same procedure as Eq. (16) derived from Eq. (13).

Fig. 11 shows the relative nonlinear parameter, $\bar{\varepsilon}/\varepsilon_0$, of a bubbly liquid as a function of the initial bubble volume fraction in mercury as well as in water. It has its maximum at a certain value of $\bar{\varepsilon}/\varepsilon_0$; that is, $(\bar{\varepsilon}/\varepsilon_0)_{\max} = 10^3$ for the case of water, and $(\bar{\varepsilon}/\varepsilon_0)_{\max} = 10^4$ for the case of mercury without surface tension, respectively. The nonlinear parameter in mercury is one order higher than that in water. When the surface tension is considered, the nonlinearity will be greatly affected in the large surface tension regime where the bubble radius is small, for example, $(\bar{\varepsilon}/\varepsilon_0)_{\max} = 10^5$ in the case of $R_0 = 1$ μm.

3.4. Nonlinear dynamic behavior in bubbly liquid

In order to know the effect of nonlinear parameters, the propagating process of waves was analyzed by Eq. (17) assuming a Gaussian distribution in the initial pressure distribution, P_0, in mercury. Fig. 12 shows the relative pressure normalized by the initial maximum pressure as a function of propagating distance, for the case without bubbles in mercury, $\bar{\varepsilon}/\varepsilon_0 = 1{:}\varepsilon_0 = 4.9$ [16]. If the Gaussian distribution is disturbed by a steep wave front, then it will become the evidence of shock wave generation. Up to 100 MPa the steep wave front does not appear but over 1 GPa a shock wave was established. If $\bar{\varepsilon}/\varepsilon_0 = 25$, a steep wave front appeared even at 100 MPa. A shock wave develops entirely when $\bar{\varepsilon}/\varepsilon_0$ is greater than 50.

Fig. 13 shows the relationship between the initial pressure defined by the appearance of a shock wave and the initial bubble volume fraction, β_0. In a bubbly liquid with 1 MPa initial pressure, a shock wave will appear when the bubble volume fraction is larger than 10^{-7}.

Fig. 14 shows the generation of a shock wave for the case of pulsed spallation in the mercury target with and

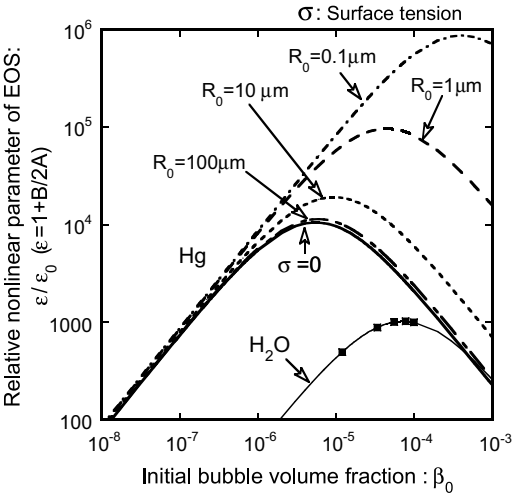

Fig. 11. Relative sound velocity vs. initial bubble volume fraction for the case of water and mercury with and without surface tension.

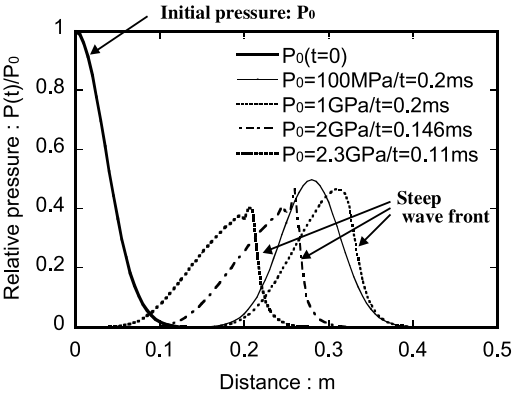

Fig. 12. Distortion of a pressure distribution accordingly to initial pressure amplitude using nonlinear second order EOS of mercury ($\varepsilon_0 = 4.9$); initial pressure distribution was Gaussian distribution.

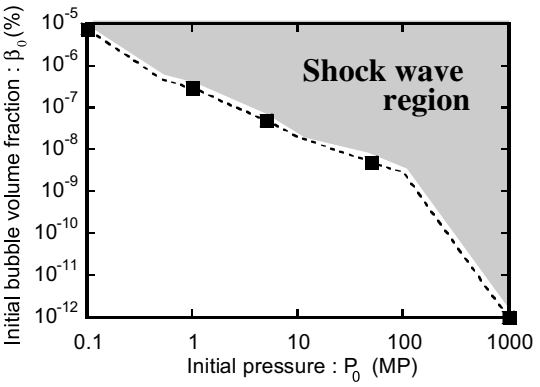

Fig. 13. Relationship between initial pressure and bubble volume fraction when distortion of initial pressure distribution occurs in mercury.

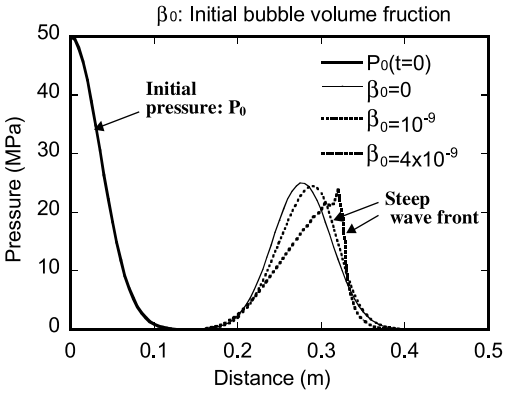

Fig. 14. Generation of a shock wave in the mercury target with and without bubbles; initial pressure distribution was Gaussian distribution with a same amplitude.

without bubbles; the pressure is about 50 MPa in mercury. The result shows the potential generation of shock wave even for an initial bubble volume fraction is as small as 10^{-9}.

Next, the initial pressure in the mercury target is discussed. The calculation model is a mercury cylinder 10 cm in diameter and 30 cm in length. Two cases are analyzed; one is a cylinder consisting of only mercury and the other one is a mercury cylinder enclosed in a steel vessel. The vessel has a 5 mm thickness at the cylinder part, 2 mm thickness at the top flat disc, and 5 mm thickness at the bottom flat disc. We used AUTODYN [20] code for analyzing the pressure wave in mercury, which can solve the interaction problem between solid and fluid. Different schemes are used, that is, FEM in solid and finite volume method (FVM) in fluid. The vessel is formulized in the Lagrange scheme and mercury in the Eulerian scheme in common variables of velocity and pressure normal direction to the boundary of both materials.

Initial pressure is given by a function of the Gaussian distribution in the radial direction and an exponential distribution in the depth direction. The maximum pressure is 50 MPa near the top disc. The equation of state in mercury is given by the second order polynomial. The initial bubble volume fraction is 10^{-7}, the relative nonlinear parameter, $\bar{\varepsilon}/\varepsilon_0$ is 10^3 and 10^4. The second order polynomial was only taken into consideration in the positive pressure regime. In the negative pressure regime linearity was kept.

Fig. 15 shows pressure as a function of time near the top disc for the case study of a mercury cylinder without the vessel. Pressure change in mercury occurs earlier with increasing nonlinear parameter. But negative pressure in the nonlinear case is smaller than the linear EOS.

Fig. 16 shows the pressure as a function of time in mercury near the top disc for the interactive cases of a mercury cylinder with the vessel. After 70 μs the pressure

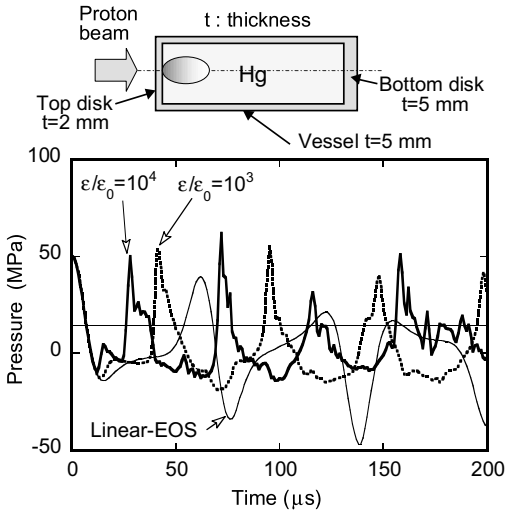

Fig. 15. Pressure as a function of time near the top disk with the rigid vessel: 300 mm length × 100 mm diameter.

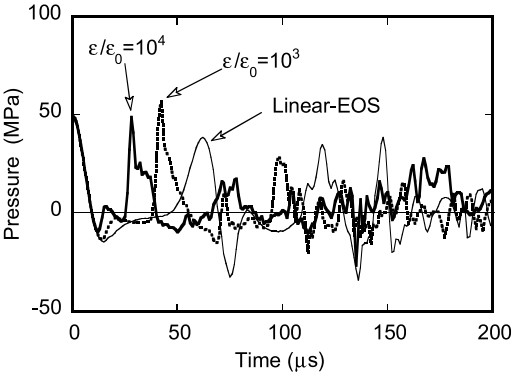

Fig. 16. Pressure as a function of time near the top disk with the elastic vessel.

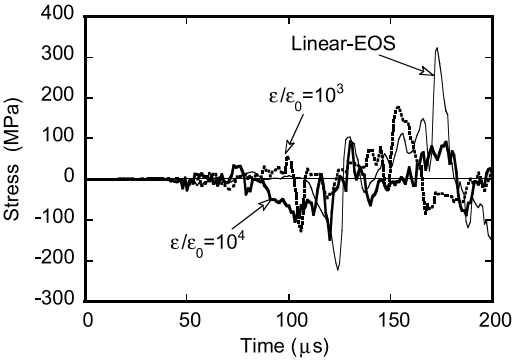

Fig. 17. Induced stress as a function of time at the center of top disk with the elastic vessel.

fluctuates more quickly and the amplitude decreased compared with those for the linear EOS. Fig. 17 shows the stress as a function of time at the center of the top disc for the interactive case of a mercury cylinder with the vessel. Induced stress decreases with increasing nonlinearity.

4. Conclusions

The thermal shock stress in the mercury target vessel was analyzed, the target receives the incident proton beam at the energy of 1 MW with the pulse duration of 1 μs. A maximum negative pressure of 61 MPa was generated following the dispersion of the compression field at 52 MPa generated in mercury. It is expected that, cavitation may be caused by the negative pressure. To understand the cavitation behavior, a simulation study was carried out using the equation of motion based on the bubble dynamics for a single bubble, and a bubbly liquid, and fundamental parameter analyses were carried out. It is found that a bubble has a potential expansion of more than 1000 times in the pressure near the window of the target vessel. Consequently wave propagation will be affected and the interaction between the vessel surface and bubble expansion must be considered.

Theoretical consideration was given to the wave motion of propagation in a bubbly liquid. The equation of state in a bubbly liquid can be approximated by a polynomial expression. This result makes general-purpose shock-analyses codes available for simulation. Analyses showed clearly that the propagation of the pressure wave would be influenced by the existence of bubbles.

In a mercury target, the inherent diameter of a bubble and the bubble volume fraction can be estimated if the critical pressure, the sound velocity, and resonance frequency are measured by static and dynamic experiments.

Acknowledgements

The authors appreciate many suggestions of Professor N. Watanabe and Dr Y. Ikeda in Japan Atomic Energy Research Institute.

References

[1] S. Ishikura, H. Kogawa, R. Hino, C. Arakawa, K. Kobayashi, R. Imai, Proc. of Computational Engineering Conference 4-5-2, 2001.
[2] L.J. Briggs, J. Appl. Phys. 24-4 (1953) 488.
[3] T.G. Leighton, The Acoustic Bubble, Academic Press, 1994.
[4] S. Fujikawa, T. Akamatsu, J. Fluid Mech. 97-3 (1980) 481.
[5] M. Shimada, Y. Matsumoto, T. Kobayashi, JSME Int. J. Ser. B 65 (1999) 634.
[6] A. Prosperetti, L.A. Crum, K.W. Commander, J. Acoust. Soc. Am. 83 (1988) 502.
[7] T. Tanahashi, Computational fluid dynamics, I.P.C, 1993.
[8] L.L. Foldy, Phys. Rev. 67 (1945) 107.
[9] L. Van Wijngaarden, Ann. Rev. Fluid Mech. 4 (1972) 369.
[10] R.E. Caflisch, M.J. Miksis, G.C. Papanicolaou, L. Ting, J. Fluid Mech. 153 (1985) 259.
[11] K.W Commander, A. Prosperetti, J. Acoust. Soc. Am. 85 (2) (1989) 732.
[12] A. Prosperetti, J. Fluid Mech. 222 (1991) 587.
[13] F.E. Fox, S.R. Curley, G.S. Larson, J. Acoust. Soc. Am. 27 (1955) 534.
[14] Yu.A. Ilinskii, E.A. Zabolotskaya, J. Acoust. Soc. Am. 92 (5) (1992) 2837.
[15] G. Du, J. Wu, J. Acoust. Soc. Am. 87 (5) (1990) 1965.
[16] M.F. Hamilton (Ed.), Nonlinear Acoustics, Academic Press, 1998.
[17] P.J. Westervelt, J. Acoust. Soc. Am. 35 (1963) 535.
[18] LS-DYNA3D Theoretical Manual, Livermore Software Technology Corporation, 1996.
[19] ABAQUS Theory Manual, Ver. 5.8, Hibbitt, Karlsson & Sorensen, Inc., 1998.
[20] AUTODYN Theory Manual, Ver. 4.1, Century Dynamics, Inc., 2000.